The Cryosphere Discuss., 6, 1037–1083, 2012
www.the-cryosphere-discuss.net/6/1037/2012/
doi:10.5194/tcd-6-1037-2012

The Cryosphere Discussions

Large sensitivity of a Greenland ice sheet model to atmospheric forcing fields

A. Quiquet[1], H. J. Punge[2], C. Ritz[1], X. Fettweis[3], M. Kageyama[2], G. Krinner[1], D. Salas y Mélia[4], and J. Sjolte[5]

[1]UJF – Grenoble 1/CNRS, Laboratoire de Glaciologie et Géophysique de l'Environnement (LGGE), UMR5183, Grenoble, 38041, France
[2]Laboratoire des Sciences du Climat et de l'Environnement (LSCE)/IPSL, CEA-CNRS-UVSQ, UMR8212, 91191 Gif-sur-Yvette, France
[3]Département de Géographie, Université de Liège, Liège, Belgium
[4]CNRM-GAME, URA CNRS-Météo-France 1357, Toulouse, France
[5]Centre for Ice and Climate, Niels Bohr Institute, Copenhagen, Denmark

Received: 13 February 2012 – Accepted: 1 March 2012 – Published: 15 March 2012

Correspondence to: A. Quiquet (aurelien.quiquet@lgge.obs.ujf-grenoble.fr)

Published by Copernicus Publications on behalf of the European Geosciences Union.

Abstract

The prediction of future climate and ice sheet evolution requires coupling of ice sheet and climate models. Before proceeding to a coupled setup, we propose to analyze the impact of model simulated climate on an ice sheet. Here, we undertake this exercise for a set of regional and global climate models. Modelled near surface air temperature and precipitation are provided as upper boundary condition to the GRISLI (GRenoble Ice Shelf and Land Ice model) hybrid ice sheet model (ISM) in its Greenland configuration.

After 20 kyr of simulation, the resulting ice sheets highlight the differences between the climate models. While modelled ice sheet sizes are generally comparable to the observed ones, there are considerable deviations among the ice sheets on regional scales. These can be explained by difficulties in modelling local temperature and precipitation near the coast. This is especially true in the case of global models. But the deviations of each climate model are also due to the differences in the atmospheric general circulation. In the context of coupling ice sheet and climate models, we conclude that appropriate downscaling methods will be needed and systematic corrections of the climatic variables at the interface may be required in some cases to obtain realistic results for the Greenland ice sheet (GIS).

1 Introduction

Recent growing consciousness of possible consequences of global warming on ice sheets (4th assessment report of the Intergovernmental Panel on climate change, IPCC-AR4, Meehl et al., 2007) motivates the use of numerical models aiming to predict their future evolution. While estimates of surface mass balance (SMB) from climate models give insights on the response of the ice sheet surface to warming climate (e.g., Yoshimori and Abe-Ouchi, 2012), ice sheet model (ISM) must be used to simulate the long term ice sheet evolution (e.g., Robinson et al., 2010). At the same time, awareness of the importance of feedbacks from other components of the Earth system has risen

TCD
6, 1037–1083, 2012

and several attempts have been undertaken to integrate ISMs into climate models in order to include and evaluate these feedback mechanisms for the upcoming centuries (Ridley et al., 2005; Vizcaíno et al., 2008, 2010). These feedbacks include, for example, water fluxes to the ocean (Swingedouw et al., 2008), orography variations (Kageyama and Valdes, 2000), and albedo changes (Kageyama et al., 2004).

However, when comparison with the real world is sought, large uncertainties remain due to shortcomings in both climate models and ISMs. Because of the long time scales involved in ice sheet development,the synchronous coupling is accessible only to low resolution and physically simplified earth system models (e.g., Fyke et al., 2011; Driesschaert et al., 2007). The direct coupling at fine resolution using a physically sophisticated atmospheric general circulation model (GCM) is still a challenge (Pollard, 2010). Recent approaches try to avoid this problem by asynchronous coupling of the climate and ISMs (Ridley et al., 2010; Helsen et al., 2011).

The recent observations of fast processes at work in the Greeland and West Antarctic ice sheets (Joughin et al., 2010) show the necessity of a synchronous coupling between ISMs representing these processes and coupled atmosphere-ocean GCMs if we want to predict the state of the ice sheets in the near future, i.e. the coming century. Relevant ISMs should include fast processes such as fast flowing ice streams and grounding line migration. These ISMs are becoming available (Ritz et al., 2001; Bueler and Brown, 2009) and a first step towards their coupling to GCM is to examine how they perform when forced by such GCM outputs. Until recently, the major concern of ISM developers was to improve the representation of physical processes occuring inside or at the boundaries of the ice sheet (e.g., Ritz et al., 1997; Tarasov and Peltier, 2002; Stone et al., 2010), primarily in order to better simulate past ice sheet evolution. In reconstructions of paleo climate, ISMs are often forced by ice core-derived proxy records, with spatial resolution of atmospheric conditions stemming from reanalysis (e.g., Bintanja et al., 2002), or from climate models snapshots (Letréguilly et al., 1991; Greve, 1997; Tarasov and Peltier, 2002; Charbit et al., 2007; Graversen et al., 2010). But for reliable projections on the future ice sheet state the explicit use of climate

TCD
6, 1037–1083, 2012

model scenarios is necessary. More specifically, a first test would be to evaluate how a Greenland ISM reacts when forced by output from different GCMs. Considering that the ablation zone extension is the more often less than 100 km (van den Broeke et al., 2008), the GCMs generally have a low resolution compared to the typical ISMs. We need consequently to assess the gain provided by higher resolution model, even if they are not global.

To date, few studies have tested the sensitivity of an ISM to atmospheric input fields explicitely. Charbit et al. (2007) showed the incapacity of an ISM forced by GCM simulations from the Paleo Climate Intercomparison Project (PMIP) to reproduce the last deglaciation of the Northern Hemisphere. The fast processes were not included in this study. Graversen et al. (2010) simulated total sea level increase over the next century using the GCMs from the Coupled Model Intercomparison Project phase 3 (CMIP-3). Here again, the fast processes were not taken into account. Neither these studies, nor more parameter-based approaches like the one of Hebeler et al. (2008), illustrate directly the links between input climate fields and simulated ice sheet behaviour. That is the main goal of the present study.

We present and discuss some of the difficulties arising when combining ice sheet and climate models. We restrict our study to the case of Greenland and choose an uncoupled approach: to examine the sensitivity of a single state of the art Greenland ice sheet (GIS) model to atmospheric input fields stemming from a number of selected climate models and, for comparison and in the tradition of previous ISM studies, a reference case derived from meteorological observations.

In Sect. 2, we first present the ISM used and its specificities. Then the choice of climate models with different degrees of resolution and comprehensiveness. The downscaling of atmospheric variables and the SMB computation is then described. Finally, ths ISM calibration and its setup for the sensitivity tests are discussed in detail. Results of the ISM simulations are shown in Sect. 3, and links between the climate model biases and horizontal resolution on the one hand and simulated deviations in ice sheet

TCD
6, 1037–1083, 2012

size and shape on the other hand are discussed. Our conclusions for future attempts of climate-ice sheet model studies are presented in Sect. 4.

2 Tools and methodology

2.1 The GRISLI ice sheet model

The model used here is a three-dimensional thermo-mechanically coupled ISM called GRISLI. Concerning ice flow dynamics, it belongs to the hybrid model type and uses both the shallow ice approximation (SIA, Hutter, 1983) and the shallow shelf approximation (SSA, MacAyeal, 1989). This model has been validated on the Antarctic ice sheet (Ritz et al., 2001; Philippon et al., 2006) and applied on the Northern Hemisphere ice sheets for paleo-climate experiments by Peyaud et al. (2007). In the more recent version used here, the association of SIA and SSA is the following:

1. A map of "allowed" ice streams is determined on the basis of basal topography. More precisely, we assume that ice streams are located in the bedrock valleys (Stokes and Clark, 1999). These valleys are derived from the difference between bedrock elevation at any given grid point and bedrock elevation smoothed over a 200-km radius around this point. Additionally, ice streams are allowed where observed present-day balance velocities are larger than $100\,\mathrm{m\,yr^{-1}}$ even if the bedrock criterion is not fulfilled.

2. Ice streams are activated only if the temperature at the ice-bed interface reaches the melting point. In this case, the SSA is used as a sliding law (Bueler and Brown, 2009). As in MacAyeal (1989), basal drag is assumed to be proportional to basal velocity; this relationship corresponds to a linear viscous sediment. In the experiments presented here, the proportionality coefficient, β, assumed to be the same for all ice streams, is one of the parameters of the model that will be calibrated by comparison with observed velocities (cf. Sect. 2.4.1).

TCD
6, 1037–1083, 2012

3. Where ice streams are not allowed or not activated, the grounded ice flow is computed using the SIA only. Ice shelves are treated with SSA only.

A specificity of the GRISLI model is the use of a polynomial constitutive equation, that adds up the Glen flow law and a Newtonian flow law to determine strain rates. This kind of law, already used in Ritz et al. (1983), accounts for the fact that the exponent of the flow law depends on the stress range (Lliboutry and Duval, 1985). Additionally, as in most large scale ISMs, we use enhancement factors that are multiplicative coefficients supposed to represent the impact of ice anisotropy on deformation. According to Ma et al. (2010), enhancement factors are different for SIA and SSA because the impact of the fabric, typically with a vertically oriented C-axis, depends on the stress regime. We thus have four different enhancement factors, for each component of the flow law (Newtonian or Glen) and for SIA and SSA (here called E_1^{SIA} and E_3^{SIA} for SIA Newtonian and Glen, respectively, and E_1^{SSA} and E_3^{SSA} for SSA Newtonian and Glen, respectively). These factors are not completely independent because the stronger a factor is for SIA, the smaller it is for SSA. These four enhancement factors are tuned in the dynamic calibration procedure (see Sect. 2.4.1 below).

The model is run on a 15-km Cartesian grid resulting from a stereographic projection with the standard parallel at 71° N and the central meridian at 39° W. The bedrock elevation map comes from the ETOPO1 dataset, which itself combines other maps (Amante and Eakins, 2009). The thickness map is derived from the work of Bamber et al. (2001); Layberry and Bamber (2001). The surface elevation is the sum of bedrock elevation and ice thickness. Figure 4 presents the initial topography. Note that under this construction there are no floating points at the time of initialization. We use the geothermal heat flux distribution proposed by Shapiro and Ritzwoller (2004). The procedure to initialize the thermal state of the ice sheet is described in Sect. 2.4.

TCD
6, 1037–1083, 2012

2.2 Climatic datasets

The ISM we use requires as input fields climatological monthly mean near surface air temperature and precipitation, as well as the model's surface topography. These are derived from a 20 yr reference period, 1980–1999, common to all models. The length of 20 yr is a compromise between the need for a meaningful climatology on the one hand and the consistency of boundary conditions used for driving the regional models and reanalysis on the other hand.

Among the CMIP-3 coupled atmosphere-ocean GCMs used for the IPCC-AR4, large discrepancies exist regarding Greenland climate (Franco et al., 2011; Yoshimori and Abe-Ouchi, 2012). We selected two models with reasonable agreement to reanalysis (Franco et al., 2011), but diverging mass balance projections in Yoshimori and Abe-Ouchi (2012):

- The coupled atmosphere-ocean GCM CNRM-CM3 (Salas-Mélia et al., 2005).
- The coupled atmosphere-ocean GCM IPSL-CM4 (Marti et al., 2010).

Surface climate fields were extracted from the CMIP-3 20th century transient simulations for years 1980 to 1999.

In addition, as an example for an atmosphere-only model with GCM resolution, we include the atmospheric component of the IPSL model, but in a version with an updated physical ice sheet surface scheme:

- The global atmosphere-only GCM LMDZ with explicit snow model adapted from the SISVAT model, as used in the regional model MAR (Brun et al., 1992; Gallée et al., 2001), termed LMDZSV. Here and for the following dataset, SST forcing used spans from 1980 to 1999.

Differing strongly from the standard-LMDZ in surface climate, this case will permit to identify the effect of an enhanced representation of surface climate processes in a GCM.

To study the impact of resolution in a GCM, we also consider:

TCD
6, 1037–1083, 2012

– The global atmosphere-only GCM LMDZ4 with an improved resolution on Greenland (Krinner and Genthon, 1998; Hourdin et al., 2006), termed LMDZZ (for zoom).

The much higher resolution over Greenland compared to IPSL-CM4 induces scaling effects of the parametrizations that lead to much different surface climate.

Regional climate models achieve much higher spatial resolutions than GCMs but require lateral boundary conditions. We selected:

– The regional climate model MAR (Fettweis, 2007; Lefebre et al., 2002). The data used stems from the 1958–2009 simulation of (Fettweis et al., 2011), forced by ERA40 as boundary conditions. We use the near surface air temperatures at the 3m level provided with the MAR output, instead of 2 m temperatures used in all other cases, but this is not likely to affect our analysis significantly.

– The regional climate model REMO (Sturm et al., 2005; Jacob and Podzun, 1997), as used in a recent isotope study on Greenland precipitation (Sjolte et al., 2011), forced by ECHAM4 as lateral boundary conditions and nudged to the upper level wind field. ECHAM4 being also here nudged towards the ERA40 wind and temperature fields every six hours. For a complete description of the nudging procedure, see Sjolte et al. (2011).

As for the GCMs, this choice is in no way meant to be complete. It was guided in part by availability of the data at the beginning of the study, but still represents the state of the art.

As example for a re-analysis, we further use:

– The reanalysis ERA40 (Uppala et al., 2005).

Finally, we include a composite data set using parameterized temperature based on geographical coordinates and altitudes together with high-resolution assimilation-based precipitation fields, which is frequently used by ice sheet modellers (e.g., Ritz et al., 1997; Greve, 2005), in our comparison. It consists in:

TCD
6, 1037–1083, 2012

– The temperature parameterization of Fausto et al. (2009) and the precipitation field of the regional model RACMO2 (Ettema et al., 2009) run with ERA40 as boundary conditions over the 1958–2009 time span. We will refer to this forcing set as FE09. The FE09 dataset was distributed by the CISM community and used e. g. in Greve et al. (2011).

From the ice sheet modelers point of view, this data set may be regarded as a reference.

The different models resolutions and external forcings are summarized in Table 1.

By construction the AOGCM simulations are the least realistic as they compute surface conditions of the atmosphere in interaction with the ocean and sea ice models and hence do not necessarily reproduce the variability of the forcing data used for the atmospheric-only models. In terms of annual mean near surface air temperature and precipitation, the climatic datasets used in this study are within the range of the CMIP-3 models but reflect the broad dispersion, as shown in Fig. 1. We have chosen to use temperature and precipitation forcing fields from different datasets. These datasets are outputs from coupled atmosphere-ocean GCMs, atmosphere-only GCMs, regional models, and reanalysis. We assume that the range of uncertainty of CMIP-3 models is a conservative estimate of the uncertainty of observed temperature and precipitation in Greenland. Figure 1 shows that the temperature spread among the datasets we selected is comparable to that of the CMIP-3 models. By contrast, the precipitation spread among the datasets we selected is smaller than that of the CMIP-3 models. Note however that the spread of the CMIP-3 ensemble is artificially enhanced by one model, which probably overestimates the total amount of precipitation over Greenland.

Figures 2 and 3 show the 1980–1999 climatological annual mean 2 m temperature and precipitation, respectively, on and around Greenland. On these figures the original polar stereographic grid was preserved for MAR and FE09; the results of the other models are presented on polar stereographic projections. Several large scale features can be seen in Fig. 2: the MAR and CNRM models have relatively low temperatures in Central and Northern Greenland, while REMO is warmer than the other models on the

TCD
6, 1037–1083, 2012

ice sheet and CNRM seems to be too warm on the southern part of the GIS. The coarse global models fail to resolve the coastal high precipitation zone (Fig. 3); however, the climate models simulate correctly a precipitation maximum in Southeastern Greenland. However, the value of this maximum is too low for MAR and ERA40, whereas CNRM is the driest model in the northern part of the GIS. Sect. 3 will show how these different climatic conditions, caused by different representations of orography and boundary conditions, but also different dynamical schemes and physical parameterizations, translate to the ice sheet properties.

2.3 SMB computation

The ISM is forced by the atmospheric fields described in Sect. 2.2. To compute the SMB, we use monthly means of temperature and precipitation for present day climate. Even if the SMB is an output of the atmospheric models, we cannot use it directly for the ISM because of the large difference in resolution between the two grids. Innovative techniques using SMB gradients exist (Helsen et al., 2011) but are stricly limited to high resolution climate models and consequently exclude GCMs. The downscaling of near surface air temperature and precipitation is physically based, as detailed below, contrary to the SMB downscaling, which is not. Thus, we compute the SMB from downscaled temperature and precipitation.

Ablation is computed with the widely-used Positive Degree Days (PDD) method (Reeh, 1991). Even if this method is a very schematic representation of surface melt (van den Broeke et al., 2010) it is still commonly used among the glaciologist community (e.g., Peyaud et al., 2007; Greve et al., 2011; Kirchner et al., 2011; Graversen et al., 2010). We compute the number of PDD, representing melt capacity, numerically at each grid point, based on the downscaled monthly mean near-surface temperature. Following Reeh (1991), a statistical temperature variation is considered, allowing melt even in months with mean temperature below the freezing point. The PDD are first used to melt the snow layer. A fraction of the melted snow is allowed to refreeze, within the limit of 60 % of solid precipitation, generating superimposed ice. The refreezing is

TCD
6, 1037–1083, 2012

responsible for firn warming, as described in Reeh (1991). Remaining PDD are used to melt possible superimposed ice from refreezing and then old ice.

The PDD integration constants and the melt rates of snow and ice are listed in Table 2. We have chosen C_{snow} to be substantially larger than in Reeh (1991). But the melting rate coefficients are poorly constrained and a wide range of values can be found in the literature (van den Broeke et al., 2010). This choice was motivated by the better agreement of ablation with the one simulated in regional models (Fettweis et al., 2011; Ettema et al., 2009).

The ISM distinguishes between rainfall and snowfall. Liquid precipitation does not contribute to the surface mass balance and is supposed to run off instaneously. This procedure is a drastic simplification, but still commonly employed (Charbit et al., 2007; Peyaud et al., 2007; Hubbard et al., 2009; Kirchner et al., 2011). An explicit refreezing model (Janssens and Huybrechts, 2000) was tested but produced only slight differences (not shown). The monthly solid precipitation, P_{sm}, is calculated based on total monthly precipitation P_{m} and monthly near surface air temperature T_{m}, following Marsiat (1994):

$$\frac{P_{\text{sm}}}{P_{\text{m}}} = \begin{cases} 0\,, & T_{\text{m}} \geq 7\,^{\circ}\text{C} \\ (7\,^{\circ}\text{C} - T_{\text{m}})/17\,^{\circ}\text{C}\,, & -10\,^{\circ}\text{C} \geq T_{\text{m}} \geq 7\,^{\circ}\text{C} \\ 1\,, & T_{\text{m}} \leq -10\,^{\circ}\text{C} \end{cases} \quad (1)$$

As the ice sheet topography changes during the simulation, and can hence differ strongly from the one prescribed in the atmospheric models, the near surface air temperature has to be adapted. For this correction we use a vertical temperature gradient, referred to hereafter as topographic lapse rate, which does not vary spatially but is different from month to month. The monthly values follow an annual sinusoidal cycle with a minimum in July at 5.426 °C km^{-1} and an annual mean of 6.309 °C km^{-1}. They are derived from the Greenland surface temperature parameterization proposed by Fausto et al. (2009). The adaptation method is thus consistent with the FE09 reference experiment. The gradients obtained in this way are derived from spatial variations of

TCD
6, 1037–1083, 2012

near surface air temperature and not from the actual temperature response to surface elevation changes at each grid point. Such an information could be obtained only by repeated atmospheric model simulations with different topographies, as performed by Krinner and Genthon (1999), who found values that are close to the ones we use here. While assuming that the sensitivity of the results to the topographic lapse rate is of second order compared with the differences among climate models at a first time, we test this hypothesis in Sect. 3.5.

The temperature field from the low resolution topography of the climate model (T_0) is downscaled to the high resolution required for the ISM (T_{ref}) using the topographic lapse rate correction as described above. For the downscaling of the precipitation rate, we used an empirical law linking temperature differences to accumulation ratio (Ritz et al., 1997):

$$\frac{P_{\text{ref}}}{P_0} = \exp(-\gamma \times (T_{\text{ref}} - T_0)), \tag{2}$$

in which the ratio of precipitation change with temperature change, γ, is poorly constrained (Charbit et al., 2002). We use a value of $\gamma = 0.07$, which corresponds to a 7.3 % change of precipitation for every 1 °C of temperature change approximately (Huybrechts, 2002).

2.4 Experimental set-up of the ice sheet model

2.4.1 Spin-up and dynamic calibration

Finding appropriate initial conditions to start the simulation of an ice sheet evolution has, for a long time, been a difficult problem. In the experiments presented here we wanted to start from fields as close as possible to the present state. The prognostic variables of ISMs are ice thickness, bedrock topography and ice temperature. The first two of them are the reasonably well-known 2-D horizontal fields (Bamber et al., 2001; Layberry and Bamber, 2001; Amante and Eakins, 2009). The 3-D temperature field is

TCD
6, 1037–1083, 2012

much more difficult to estimate but is also crucial because it is strongly linked to the velocity distribution. The temperature distribution within the ice depends on the past evolution of the ice sheet, in particular on past boundary conditions including surface mass balance and near surface air temperature. The typical time scale of thermal processes is up to 20 kyr (Huybrechts, 1994), so today's ice temperature is still affected by the last deglaciation.

To account for this past evolution, we run a long glacial-interglacial spin-up simulation to obtain a realistic present temperature field. To do so, we use present-day climatic conditions and apply perturbations deduced from proxy-data. The present day atmospheric fields of temperature and precipitation are the same as in the FE09 experiment.

The temperature anomalies with respect to present-day were reconstructed following Huybrechts (2002) based on the GRIP isotopic record (Dansgaard et al., 1993; Johnsen et al., 1997). These time-dependent anomalies are used as deviations from present-day conditions to force the ISM. The resulting precipitation anomalies are assumed to follow the temperature evolution as in Eq. (2).

However the 3-D temperature field obtained after this spinup procedure is associated with a topography different from the observed one. Consequently, for the sensitivity experiments, we stretch the temperature field to the observed topography in order to obtain the initial state.

Once the 3-D temperature field has been obtained, we perform a dynamic calibration to tune the various parameters that govern the velocity field. These are the four enhancement factors and the β coefficient of the basal drag presented in Sect. 2.1. Assuming that after the spinup procedure the temperature field is realistic, the velocity field will depend on these parameters only. Our target is the surface velocity field measured by radar interferometry (Joughin et al., 2010).

We must stress that for ice streams, it is almost impossible to tune the coefficient β of basal drag and the enhancement factors E_1^{SSA} and E_3^{SSA} separately. As explained in Sect. 2.1, the SIA and SSA enhancement factors are not independent and we added a constraint on the relationship between SIA and SSA. This is because the

TCD
6, 1037–1083, 2012

enhancement factors are both equal to 1.0 in the case of isotropic ice, and stronger the ice anisotropy, the higher the SIA enhancement factors and the lower the SSA enhancement factors (Ma et al., 2010). We chose $E^{SSA} = 0.9$ for $E^{SIA} = 2.0$, $E^{SSA} = 0.8$ for $E^{SIA} = 3.0$, $E^{SSA} = 0.63$ for $E^{SIA} = 5.0$. The procedure consists in running short (100 yr) simulations in a constant present-day climate. We ran a matrix of simulations by varying simultaneously and independently the five parameters already mentioned: the enhancement factors E_1^{SSA}, E_3^{SSA}, E_1^{SIA} and E_3^{SIA}, and the β coefficient of basal drag. The range tested for the SIA enhancement factors was $1.0 < E^{SIA} < 5.0$, corresponding to SSA factors of $1.0 > E^{SIA} > 0.63$. The range tested for the β coefficient was 500 to 1500 Pa yr m^{-1}. For each set of parameters, we computed mean squared error and standard deviation, in terms of difference between observed and simulated velocities as well as in terms of the respective flux of ice (being the velocity multiplied by the ice depth). The best set of parameters corresponds to the minimum on those quantities. Considering that a different set of parameters can give us approximately the same statistical scores, we also examined at the distribution of velocity amplitudes. The set of parameters which gave the best agreement with the observed velocity amplitudes plotted onto an histogram was selected.

This best set obtained was with:

- Glen cubic law: $E_3^{SIA} = 3.0$ and $E_3^{SSA} = 0.8$.
- Newtonian finite viscosity: $E_1^{SIA} = 1.0$ and $E_1^{SSA} = 1.0$.
- Coefficient of the basal drag: $\beta = 1500$ Pa yr m^{-1}.

These values are consistent with the findings of Ma et al. (2010), and with the range 3.0–5.0 generally used in the SIA and Glen flow law case. We use this set of parameters in all further experiments.

This solution is not unique, because we can obtain the same velocity field with more viscous ice streams (lower SSA enhancement factor) and weaker basal drag. Our calibration is also strongly dependent on the initial temperature field, which is in turn greatly

TCD
6, 1037–1083, 2012

affected by the poorly constrained distribution of geothermal heat flux (Greve, 2005). But our sensitivity studies indicate that the model results are much more sensitive to surface mass balance than to dynamic parameters: with the FE09 forcing, a doubling of sliding ($\beta/2$) induce a 0.1 % of total volume reduction, while changing the FE09 forcing for the MAR forcing induces a 9.0 % of total volume increase.

2.4.2 Sensitivity test procedure

Having calibrated the dynamical parameters, we perform the comparison of the responses to climate model forcings. We keep the same set of dynamic and mass balance downscaling parameters in all the experiments, and change only the atmospheric fields of total precipitation and near surface air temperature provided by the atmospheric models. We then run 20 kyr-long experiments to allow for the ice sheet to stabilize, keeping the climate constant over time ("glaciological steady state"). Nevertheless, during those simulations, temperature, and consequently precipitation, is likely to change, in relation with the elevation changes as described in Sect. 2.3. Due to the temperature memory effect mentioned above, we cannot expect to simulate the present observed topography. In a way this type of experiment is closer to a future projection experiment. The focus of our analysis in Sect. 3 will thus be on the range of relative deviation, from the present reference state obtained with the different climatic forcings.

3 Results

3.1 20 kyr equilibrium simulated topographies

Figure 5 presents the impact of inter-model climate differences in terms of simulated topography at the end of the run. Differences between simulated topographies and observed topography is available in the supplementary material accompanying this paper. A remarkable diversity of simulated topographies is observed. At first sight, the

TCD
6, 1037–1083, 2012

southern part of the ice sheet is more stable than the northern part. In the North, at the end of the simulation, with two models (REMO and ERA40) presenting almost no ice, and at least three models (CNRM, MAR, IPSL) presenting a fully covered area, the range is very broad. The surface height is also very different among the models with an approximate 7 % thickening for MAR in the interior and 8 % thinning with IPSL. In all the simulations, the ice sheet is spreading towards the South West. This common feature is due to the incapacity of the ISM to reproduce fine scale features. The South of Greenland is indeed a very mountainous area characterised by large orographic precipitation and high slope effects, even in the ice flow dynamics. The 15-km grid is too coarse to reproduce such local effects and specific parameterizations would be needed (Marshall and Clarke, 1999).

To distinguish between the different regional behaviours we consider three regions: a southern region with latitudes lower than 68° N, a northern one with latitudes greater than 75° N, and a central region in between. Specific differences occur mainly in the North and in the South. The central region presents a more complex response and we were not able to identify well-defined specificities. Hence, in general, we discuss here only the results for the South and North regions. The evolution of the simulated volume for the northern and southern regions is presented in Figs. 6a and 7a, respectively. Except for MAR and CNRM experiments, all models simulate a decrease of ice volume in the North. If we put aside REMO and ERA40, which simulate nearly no ice in this region, the volume variation ranges from -0.1 to $+0.16 \times 10^6$ km^3 in 20 kyr. REMO and ERA40 present the same pattern of retreat probably due to the nudging procedure of the REMO model towards the ERA40 reanalysis. The southern region systematically gains ice volume (Fig. 7a), and the response of the ISM is almost instantaneous, compared to typical evolution time scales, given that 50 % of the final volume variation is generally achieved in a thousand years. The volume simulated by all models reaches a maximum before decreasing slightly due to the precipitation correction. The final volume deviation in this region ranges from 0.05 to 0.15 $\times 10^6$ km^3 in 20 kyr.

TCD
6, 1037–1083, 2012

3.2 Comparisons of the atmospheric model results to observation and link with the ISM response

The simulated topographies presented in Fig. 5 and the simulated regional volume evolutions presented in Figs. 6a and 7a highlight the spread of results due to different atmospheric inputs. In this section, we study the simulated volume deviation, by comparing the atmospheric datasets on local and regional scales. We take advantage of the presence of weather stations in Greenland to validate the atmospheric near surface temperature fields in the datasets at selected points.

Near surface air temperatures for each atmospheric model and for observations are plotted in Figs. 6 and 7c,d. Station 2 m temperature data is evaluated for the automated weather stations (AWS) Humboldt, TUNU-N and South Dome located on the GIS (Steffen et al., 1996) and for the coastal DMI station in Nuuk (Cappelen et al., 2011). For precipitation, Figs. 6 and 7b, we compare regional means.

The location of the stations is indicated in Fig. 4. At the Humboldt AWS in the Northwest of the ice sheet (Fig. 6c), it is apparent that temperatures simulated by ERA40 and REMO are around 5 °C too high compared to observations climatological mean in July. This is certainly the main reason for the rapid ice retreat in this region for those models. The IPSL and LMDZZ models are also slightly warmer than observations in summer, while their seasonal cycle appears to be delayed by a few weeks. MAR is too cold throughout the year. There is a spread among models in winter, and the sinusoidal constructed FE09 is not satisfactory for boreal winter, but these deficiencies are not relevant for melt and are certainly less significant for the ice mass balance than summer is. At the same time, the IPSL model is too warm in particular during boreal winter but also on average, which favours a more rapid ice movement and hence a rather thin ice sheet in the region despite displaying the highest precipitation of all models.

At the more eastern TUNU-N station, the warm bias of REMO and ERA40 is confirmed. Precipitation is relatively low for the LMDZZ, LMDZSV and CNRM models, but

TCD
6, 1037–1083, 2012

for the latter this bias has no impact on the ice sheet thickness because a strong cold bias from November through July eventually reduces the summer melt.

At Summit (not shown), the spread of model temperatures in summer has certainly less of an impact due to the absence of melting. LMDZZ and IPSL have the lowest precipitation, resulting in a relatively low ice surface elevation. In contrast, the high precipitation models CNRM and, in particular, MAR have a thicker ice sheet.

At South Dome, the IPSL and CNRM models show strong warm biases, by up to 15 °C, and a too small annual cycle. At the same time, they have much higher precipitation than the other models. This can certainly partly be explained by the very coarse resolution of these GCMs, that do not capture the high topography of the dome in a satisfactory way. The IPSL model also presents a storm-tracks slightly shifted southward (Marti et al., 2010), resulting in wet bias in the south and dry bias in the north. The rather low ice sheet thickness with LMDZZ can be explained by the low precipitation in the south region in this model. LMDZZ is drier at high elevation than the IPSL probably due to resolution effects (Krinner and Genthon, 1998). However, the local comparison of atmospheric variables is not sufficient to explain the ISM response. The ice flow dynamics also have an impact on the ISM response, and local atmospheric differences at locations other than the three stations considered above may have a regional impact. The following section deals with this issue.

3.3 Sensitivity to temperature and precipitation

In the following we consider the FE09 dataset as a reference. Given that the Ettema et al. (2009) precipitation field is the output from an atmospheric model, we do not pretend here that the FE09 is the best atmospheric dataset and that it is not free of biases. The accumulation field computed from each atmospheric dataset by the ISM method after downscaling to the ISM grid was compared with the accumulation map based on ice/firn cores and coastal precipitation record of Burgess et al. (2010) and van der Veen et al. (2001). The FE09 experiment presents a better agreement than the other datasets (see Fig. 8). At this point, it should be noted that the Burgess et al.

TCD
6, 1037–1083, 2012

(2010) and van der Veen et al. (2001) accumulation field is not suitable for an ISM forcing for paleo experiments and for mid/long-term future projections. Although we have some confidence in temperature anomalies (e.g. isotopic content), accumulation is less constrained, being a joint result of both near surface air temperature and precipitation. Differences between each individual atmospheric dataset and the FE09 dataset in term of July temperature and annual mean precipitation on the ISM grid are available in the supplementary material.

Considering that ISM dynamical parameters and basal conditions are identical in all simulations, the spread of resulting topographies only results from differences in near surface air temperature and precipitation. In order to distinguish the effect of the two fields, we repeated the previous standard experiments (Table 1), but replaced the precipitation fields by the reference of Ettema et al. (2009). Thus, in the following, the terms "too cold/warm/dry/wet" refer to the deviation from this simulation.

This approach is different from the simple comparison for all atmospheric models as performed in the previous section because it enables us to compare the atmospheric differences in terms of ice-sheet response. For example, a warm bias at an ice stream terminus is likely to have a higher impact than the same bias in a slowly moving area. Thus, this section first aims at measuring the impact of the regional differences of climate models from a glaciological point of view. We also aim at determining the key variable (temperature or precipitation) explaining the spread of ISM simulated volume amongst the atmospheric models.

Let us note dV_0, the volume variation (simulated minus present day observations) at the end of the 20 kyr FE09 simulation. For each atmospheric model i of Table 1, let us note dV_i, the volume variation of the standard ISM experiment and dV_i', the volume variation for the simulation where precipitation fields have been replaced by the one of Ettema et al. (2009).

Given these anomalies of volume, six cases are possible. The first family of results corresponds to a standard simulated volume lower than the reference, $dV_i < dV_0$. This

TCD
6, 1037–1083, 2012

negative anomaly can be due to conditions which are too dry or/and too warm. Three sub cases can be identified:

- $dV_i < dV_i' < dV_0$: the use of the Ettema et al. (2009) precipitation map increases the simulated volume, which however stays below the reference one. The considered dataset is consequently too dry ($dV_i' > dV_i$) but also too warm ($dV_0 > dV_i'$).
- $dV_i < dV_0 < dV_i'$: as for the previous case, the use of the Ettema et al. (2009) precipitation map increases the simulated volume, but here the final volume anomaly is greater than the reference one. The considered dataset is consequently too dry ($dV_i' > dV_i$) and too cold ($dV_i' > dV_0$).
- $dV_i' < dV_i < dV_0$: the simulated volume is even lower with the use of the Ettema et al. (2009) precipitation map. The considered dataset is consequently too wet ($dV_i > dV_i'$) and too warm ($dV_0 > dV_i'$). This case indicates a much warmer atmospheric model, because even if it is wetter, the ISM simulated volume is still below the reference volume.

The second family of results corresponds to a simulated volume greater than the reference, $dV_i > dV_0$. This negative anomaly can be due to too wet conditions or/and to too cold conditions. Again three sub cases can be identified:

- $dV_i' > dV_i > dV_0$: the use of the Ettema et al. (2009) precipitation map increases the simulated volume, enhancing the positive volume anomaly. The considered dataset is consequently too dry ($dV_i' > dV_i$) and too cold ($dV_i' > dV_0$). Note that this case suggests that the atmospheric model is strongly cold biased, because even if it is drier, the ISM simulated volume is still above the reference volume.
- $dV_i > dV_i' > dV_0$: in this case, the use of the Ettema et al. (2009) precipitation map decreases the simulated volume, which still stays however above the reference level. The considered dataset is consequently too wet ($dV_i > dV_i'$) and too cold ($dV_i' > dV_0$).

TCD
6, 1037–1083, 2012

– $dV_i > dV_0 > dV_i'$: as for the previous case, the use of the Ettema et al. (2009) precipitation map decreases the simulated volume, which becomes lower than the reference one. The considered dataset is consequently too wet ($dV_i > dV_i'$) and too warm ($dV_0 > dV_i'$).

The relative importance of temperature and precipitation can be evaluated considering the difference between the simulated volumes. When the value of dV_i' is close enough to dV_0, it means the precipitation is the key factor, and temperature is secondary. On the other hand, when dV_i' and dV_i are similar, temperature has to be considered as the key factor.

According to this classification and with the simulated volume variations plotted in Fig. 9, we can identify the main bias of the atmospheric models in terms of glaciological response and the key variable for the North and South regions (see Table 3).

The warm models generally retreat in the North, even if they often present a relatively high anomaly of precipitation. For instance, the two models presenting a collapse of the northern part, ERA40 and REMO, present a warm bias and the deviation of volume is attributable to the temperature only. It seems that the deviation of volume amongst the models is mainly attributable to air temperature in the North (3 out of 8 cases for near surface temperature, 0 out of 8 for precipitation) and precipitation in the South (3 out of 8 for precipitation, 1 out of 8 for near surface temperature).

Hence the northern region appear as highly sensitive to air temperature and is proner to large volume changes than the southern region. Therefore, we want to investigate whether a given warm bias in the North is equivalent to the same given warm bias in the South. This question is investigated in the next section.

3.4 Sensitivity of the ISM to the July temperature

Figure 10 presents the anomaly of gained and lost volume for the different regions against the mean July temperature in the corresponding region for each of the eight forcing datasets. We distinguish short-term (500 yr) and long-term responses (20 kyr)

TCD
6, 1037–1083, 2012

in volume anomaly. Each position on the temperature axis corresponds to a specific climatic dataset. There is a wide spread in North region temperature among the models: the range of the simulated temperatures over the northern region is 10 °C, while it is less than 5 °C for the southern region. In the South for both short-term and long-term response, the volume loss, which is close to 0 in most cases, is insensitive to an increase in temperature. The volume gain in this region, however, increases with rising temperatures on the short-term, but decreases slightly with increasing temperatures on the long-term.

In the North, for both the short-term and long-term responses, an increase of mean July temperature implies a decrease of volume gain and increase of volume loss. In the long-term response, we can observe a kind of threshold on the July temperature around −2 °C, above which the volume loss increases drastically. The medium region is intermediate, responding more like the North in the short-term and more like the South for the volume loss in the long-term.

3.5 Sensitivity to topographic lapse rate

Independently from the climatic datasets, we have also tested the effect of the altitude-temperature-precipitation feedback. We performed again the set of 8 experiments (Table 1) in the exact same conditions, except that the lapse rate correction is switched off. In these conditions, temperature and precipitations stay constant during all of the simulation.

The evolution of the difference of ice volume in the no-lapse rate experiment with respect to the standard correction experiment for South and North regions is presented in Fig. 11. The two regions present a completely different response.

In the South, all the models present a lower value of the volume anomaly in the no-lapse rate experiment than in the standard one. Considering that this volume anomaly is systematically positive in this region (see Fig. 7a), the no-lapse rate experiments present a better agreement with the initial state. As we already mentioned, the ISM is not adapted to reproduce steep slopes such as those observed in the South. The

TCD
6, 1037–1083, 2012

resulting spread leads to an increase of the elevation in the peripheral area, initially in the ablation zone, but with a high value of precipitation. With the topographic lapse rate correction, the ISM turns this warm very high precipitation zone into a mild/cold high precipitation zone. The resulting displacement of the equilibrium line is hence a direct consequence of the downscaling method and of the resolution of the ISM.

In the North, all the simulations present a bigger ice sheet in the no-lapse rate experiment. The only exception is IPSL, i.e. the only model that retreats and has a cold and dry bias. For this model, the dry anomaly causes a global thinning of the ice sheet. A warming and a consequent increase of precipitation is observed when the feedback is taken into account. Two experiments (REMO and ERA40) present a huge difference between no-lapse rate and standard experiment. Those two models present a collapse of the North of the GIS (see Fig. 6a) in the standard experiment but in the no-lapse rate, the ice sheet stabilises and is still present at the end of the run. The lapse rate correction accelerates and thus accentuates the retreat.

The datasets presenting a volume increase in the North (MAR and CNRM) produce a slightly bigger volume when the feedback is switched-off. This is mainly due to the cold bias already in those datasets (see Sect. 3.3), allowing an advance of the ice over what is normally tundra zone.

We can conclude that the lapse rate correction is an important driver for the datasets with temperature as a predominant variable, accentuating the biases (North case). However, when precipitation is the driver, the lapse rate correction tends to reduce the deviation (South case). It also appears that we cannot neglect the topographic correction for simulations lasting more than a thousand years.

4 Conclusions

In face of the uncertainties on future climate, we need to develop tools to predict the coupled climate ice sheet evolution for the coming centuries. A first step in this development should be the validation of the uncoupled approach and to do so, we have

TCD
6, 1037–1083, 2012

proposed here a sensitivity study of an ice sheet model (ISM) to atmospheric fields. We have applied several climatic datasets as climate forcing to an ISM in climatic steady state experiments. We have shown major discrepancies in the resulting simulated ice sheets due to the tendency of the ISM to integrate the biases in the atmospheric forcings. Apart from the numerical and physical differences among the climate models, the model resolution also has an impact on the biases of the analyzed cases. With the ISM presented here, which implies an interpolation of the forcing fields, we do not find a systematic difference between regional climate models and global GCMs. Nonetheless, some models seem to be inappropriate for absolute forcing. For these models, we suggest the use of an anomaly method, in which the ISM is forced with the best available present day climatology plus anomalies computed by the climate model as a perturbation, instead.

Although July temperature seems to be the major driver of the ISM behaviour, in particular in the northern part of the GIS, precipitation may also play an important role, in particular in the South. We have shown that the North of Greenland is more sensitive to temperature anomalies than the South and we suspect that major changes are likely to occur there in a warmer climate. The South seems to be relatively stable and almost insensitive to July temperature. This conclusion is in contradiction with the works of Cuffey and Marshall (2000); Otto-Bliesner et al. (2006); Robinson et al. (2010), but well agree with Stone et al. (2010); Greve et al. (2011); Born and Nisancioglu (2011); Fyke et al. (2011). The discrepancy between the definition of the sensitive region may be due to the SMB calulation procedure employed, the PDD method enhancing the changes in a warmer climate compared to more physically based calculation (Solgaard and Langen, 2012). The bedrock map used can also greatly affect the results (Stone et al., 2010).

The topographic lapse rate of the ISM atmospheric correction can play an important role in simulations lasting several thousand years, even though it is of second order compared to atmospheric model biases. The current ISM is unable to reproduce precisely the southern ice sheet topography because it does not take the very fine scale

TCD
6, 1037–1083, 2012

processes occuring in this region into account. To improve on this, the ISM requires very fine resolution atmospheric forcing fields and the use of better downscaling techniques (as proposed by Gallée et al., 2011).

Supplementary material related to this article is available online at: http://www.the-cryosphere-discuss.net/6/1037/2012/tcd-6-1037-2012-supplement.pdf.

Acknowledgements. We thank CISM for providing the datasets of Shapiro and Ritzwoller (2004); Joughin et al. (2010); Burgess et al. (2010); van der Veen et al. (2001). Janneke Ettema, Jan van Angelen and Michiel van den Broeke (IMAU, Utrecht University) are thanked for providing RACMO2 climate fields. We thank Konrad Steffen and the DMI for providing temperature data for the Greenland weather stations. Aurélien Quiquet is supported by the ANR project NEEM-France. NEEM is directed and organized by the Center of Ice and Climate at the Niels Bohr Institute and US NSF, Office of Polar Programs. It is supported by funding agencies and institutions in Belgium (FNRS-CFB and FWO), Canada (NRCan/GSC), China (CAS), Denmark (FIST), France (IPEV, CNRS/INSU, CEA and ANR), Germany (AWI), Iceland (RannIs), Japan (NIPR), Korea (KOPRI), The Netherlands (NWO/ALW), Sweden (VR), Switzerland (SNF), UK (NERC) and the USA (US NSF, Office of Polar Programs). Heinz-Jürgen Punge is supported by the european commission FP7 project 226520 COMBINE and the ANR project NEEM-France. This work was supported by funding from the ice2sea programme from the European Union 7th Framework Programme, grant number 226375. Ice2sea contribution number ice2sea066.

The publication of this article is financed by CNRS-INSU.

TCD
6, 1037–1083, 2012

References

Amante, C. and Eakins, B.: ETOPO1 1 Arc-Minute Global Relief Model: Procedures, Data Sources and Analysis, NOAA Technical Memorandum NESDIS NGDC-24, p. 19, 2009. 1042, 1048

Bamber, J. L., Layberry, R. L., and Gogineni, S. P.: A new ice thickness and bed data set for the Greenland ice sheet 1. Measurement, data reduction, and errors, J. Geophys. Res., 106, 33773–33780, doi:10.1029/2001JD900054, 2001. 1042, 1048

Bintanja, R., van de Wal, R. S. W., and Oerlemans, J.: Global ice volume variations through the last glacial cycle simulated by a 3-D ice-dynamical model, Quatern. Int., 95-96, 11–23, doi:10.1016/S1040-6182(02)00023-X, 2002. 1039

Born, A. and Nisancioglu, K. H.: Melting of Northern Greenland during the last interglacial, The Cryosphere Discuss., 5, 3517–3539, doi:10.5194/tcd-5-3517-2011, 2011. 1060

Brun, E., David, P., Sudul, M., and Brunot, G.: A numerical model to simulate snow-cover stratigraphy for opera tional avalanche forecasting, J. Glaciol., 38, 13–22, 1992. 1043

Bueler, E. and Brown, J.: Shallow shelf approximation as a "sliding law" in a thermomechanically coupled ice sheet model, J. Geophys. Res., 114, F03008, doi:10.1029/2008JF001179, 2009. 1039, 1041

Burgess, E. W., Forster, R. R., Box, J. E., Mosley-Thompson, E., Bromwich, D. H., Bales, R. C., and Smith, L. C.: A spatially calibrated model of annual accumulation rate on the Greenland Ice Sheet (1958–2007), J. Geophys. Res.-Earth, 115, F02004, doi:10.1029/2009JF001293, 2010. 1054, 1061, 1080

Cappelen, J., Laursen, E. V., Jørgensen, P. V., and Kern-Hansen, C.: DMI Monthly Climate Data Collection 1768-2009, Denmark, The FaroeIslands and Greenland, DMI Technical Report, 10-05, 2011. 1053

Charbit, S., Ritz, C., and Ramstein, G.: Simulations of Northern Hemisphere ice-sheet retreat: sensitivity to physical mechanisms involved during the Last Deglaciation, Quatern. Sci. Rev., 21, 243–265, doi:10.1016/S0277-3791(01)00093-2, 2002. 1048

Charbit, S., Ritz, C., Philippon, G., Peyaud, V., and Kageyama, M.: Numerical reconstructions of the Northern Hemisphere ice sheets through the last glacial-interglacial cycle, Clim. Past, 3, 15–37, doi:10.5194/cp-3-15-2007, 2007. 1039, 1040, 1047

Cuffey, K. M. and Marshall, S. J.: Substantial contribution to sea-level rise during the last interglacial from the Greenland ice sheet, Nature, 404, 591–594, 2000. 1060

TCD
6, 1037–1083, 2012

Dansgaard, W., Johnsen, S. J., Clausen, H. B., Dahl-Jensen, D., Gundestrup, N. S., Hammer, C. U., Hvidberg, C. S., Steffensen, J. P., Sveinbjornsdottir, A. E., and Jouzel, J.: Evidence for general instability of past climate from a 250-kyr ice-core record, Nature, 364, 218–220, 1993. 1049

Driesschaert, E., Fichefet, T., Goosse, H., Huybrechts, P., Janssens, I., Mouchet, A., Munhoven, G., Brovkin, V., and Weber, S. L.: Modeling the influence of Greenland ice sheet melting on the Atlantic meridional overturning circulation during the next millennia, Geophys. Res. Lett., 34, L10707, doi:10.1029/2007GL029516, 2007. 1039

Ettema, J., van den Broeke, M. R., van Meijgaard, E., van de Berg, W. J., Bamber, J. L., Box, J. E., and Bales, R. C.: Higher surface mass balance of the Greenland ice sheet revealed by high-resolution climate modeling, Geophys. Res. Lett., 36, L12501, doi:10.1029/2009GL038110, 2009. 1045, 1047, 1054, 1055, 1056, 1057, 1070, 1081

Fausto, R. S., Ahlstrøm, A. P., van As, D., Bøggild, C. E., and Johnsen, S. J.: A new present-day temperature parameterization for Greenland, J. Glaciol., 55, 95–105, doi:10.3189/002214309788608985, 2009. 1045, 1047, 1070

Fettweis, X.: Reconstruction of the 1979–2006 Greenland ice sheet surface mass balance using the regional climate model MAR, The Cryosphere, 1, 21–40, doi:10.5194/tc-1-21-2007, 2007. 1044, 1070

Fettweis, X., Tedesco, M., van den Broeke, M., and Ettema, J.: Melting trends over the Greenland ice sheet (1958–2009) from spaceborne microwave data and regional climate models, The Cryosphere, 5, 359–375, doi:10.5194/tc-5-359-2011, 2011. 1044, 1047

Franco, B., Fettweis, X., Erpicum, M., and Nicolay, S.: Present and future climates of the Greenland ice sheet according to the IPCC AR4 models, Clim. Dynam., 36, 1897–1918, doi:10.1007/s00382-010-0779-1, 2011. 1043

Fyke, J. G., Weaver, A. J., Pollard, D., Eby, M., Carter, L., and Mackintosh, A.: A new coupled ice sheet/climate model: description and sensitivity to model physics under Eemian, Last Glacial Maximum, late Holocene and modern climate conditions, Geosci. Model Dev., 4, 117–136, doi:10.5194/gmd-4-117-2011, 2011. 1039, 1060

Gallée, H., Guyomarc'h, G., and Brun, E.: Impact of snow drift on the Antarctic ice sheet surface mass balance: possible sensitivity to snow-surface properties, Bound.-Lay. Meteorol., 99, 1–19, 2001. 1043

Gallée, H., Agosta, C., Gential, L., Favier, V., and Krinner, G.: A downscaling approach toward high-resolution surface mass balance over Antarctica, Surv. Geophys., 32, 507–518,

TCD
6, 1037–1083, 2012

doi:10.1007/s10712-011-9125-3, 2011. 1061
Graversen, R. G., Drijfhout, S., Hazeleger, W., van de Wal, R., Bintanja, R., and Helsen, M.: Greenland's contribution to global sea-level rise by the end of the 21st century, Clim. Dynam., 37, 1427–1442, 2010. 1039, 1040, 1046
Greve, R.: Application of a polythermal three-dimensional ice sheet model to the Greenland ice sheet: Response to steady-state and transient climate scenarios, J. Climate, 10, 901–918, doi:10.1175/1520-0442(1997)010<0901:AOAPTD>2.0.CO;2, 1997. 1039
Greve, R.: Relation of measured basal temperatures and the spatial distribution of the geothermal heat flux for the Greenland ice sheet, Ann. Glaciol., 42, 424–432, 2005. 1044, 1051
Greve, R., Saito, F., and Abe-Ouchi, A.: Initial results of the SeaRISE numerical experiments with the models SICOPOLIS and IcIES for the Greenland ice sheet, Ann. Glaciol., 52, 23–30, 2011. 1045, 1046, 1060
Hebeler, F., Purves, R. S., and Jamieson, S. S. R.: The impact of parametric uncertainty and topographic error in ice-sheet modelling, J. Glaciol., 54, 899–919, 2008. 1040
Helsen, M. M., van de Wal, R. S. W., van den Broeke, M. R., van de Berg, W. J., and Oerlemans, J.: Towards direct coupling of regional climate models and ice sheet models by mass balance gradients: application to the Greenland Ice Sheet, The Cryosphere Discuss., 5, 2115–2157, doi:10.5194/tcd-5-2115-2011, 2011. 1039, 1046
Hourdin, F., Musat, I., Bony, S., Braconnot, P., Codron, F., Dufresne, J., Fairhead, L., Filiberti, M., Friedlingstein, P., Grandpeix, J., Krinner, G., Levan, P., Li, Z., and Lott, F.: The LMDZ4 general circulation model: climate performance and sensitivity to parametrized physics with emphasis on tropical convection, Clim. Dynam., 27, 787–813, doi:10.1007/s00382-006-0158-0, 2006. 1044
Hubbard, A., Bradwell, T., Golledge, N., Hall, A., Patton, H., Sugden, D., Cooper, R., and Stoker, M.: Dynamic cycles, ice streams and their impact on the extent, chronology and deglaciation of the British-Irish ice sheet, Quaternary Sci. Rev., 28, 758–776, 2009. 1047
Hutter, K.: Theoretical glaciology: material science of ice and the mechanics of glaciers and ice sheets, Springer, Reidel Publishing Company, Dordrecht, The Netherlands, 1983. 1041
Huybrechts, P.: The present evolution of the Greenland ice sheet: an assessment by modelling, Global Planet. Change, 9, 39–51, doi:10.1016/0921-8181(94)90006-X, 1994. 1049
Huybrechts, P.: Sea-level changes at the LGM from ice-dynamic reconstructions of the Greenland and Antarctic ice sheets during the glacial cycles, Quatern. Sci. Rev., 21, 203–231, doi:10.1016/S0277-3791(01)00082-8, 2002. 1048, 1049

TCD
6, 1037–1083, 2012

Jacob, D. and Podzun, R.: Sensitivity studies with the regional climate model REMO, Meteorol. Atmos. Phys., 63, 119–129, doi:10.1007/BF01025368, 1997. 1044
Janssens, I. and Huybrechts, P.: The treatment of meltwater retardation in mass-balance paramete rizations of the Greenland ice sheet, Ann. Glaciol., 31, 133–140, 2000. 1047
Johnsen, S. J., Clausen, H. B., Dansgaard, W., Gundestrup, N. S., Hammer, C. U., Andersen, U., Andersen, K. K., Hvidberg, C. S., Dahl-Jensen, D., Steffensen, J. P., Shoji, H., Árny E. Sveinbjörnsdóttir, White, J., Jouzel, J., and Fishe, D.: The δ^{18}O record along the Greenland Ice Core Project deep ice core and the problem of possible Eemian climatic instability, J. Geophys. Res., 102, 26397–26410, doi:10.1029/97JC00167, 1997. 1049
Joughin, I., Smith, B. E., Howat, I. M., Scambos, T., and Moon, T.: Greenland flow variability from ice-sheet-wide velocity mapping, J. Glaciol., 56, 415–430, doi:10.3189/002214310792447734, 2010. 1039, 1049, 1061
Kageyama, M. and Valdes, P. J.: Impact of the North American ice-sheet orography on the Last Glacial Maximum eddies and snowfall, Geophys. Res. Lett., 27, 1515–1518, doi:10.1029/1999GL011274, 2000. 1039
Kageyama, M., Charbit, S., Ritz, C., Khodri, M., and Ramstein, G.: Quantifying ice-sheet feedbacks during the last glacial inception, Geophys. Res. Lett., 31, 24203, 2004. 1039
Kirchner, N., Greve, R., Stroeven, A. P., and Heyman, J.: Paleoglaciological reconstructions for the Tibetan Plateau during the last glacial cycle: evaluating numerical ice sheet simulations driven by GCM-ensembles, Quaternary Sci. Rev., 30, 248–267, 2011. 1046, 1047
Krinner, G. and Genthon, C.: GCM simulations of the Last Glacial Maximum surface climate of Greenland and Antarctica, Clim. Dynam., 14, 741–758, doi:10.1007/s003820050252, 1998. 1044, 1054, 1070
Krinner, G. and Genthon, C.: Altitude dependence of the ice sheet surface climate, Geophys. Res. Lett., 26, 2227–2230, doi:10.1029/1999GL900536, 1999. 1048
Layberry, R. L. and Bamber, J. L.: A new ice thickness and bed data set for the Greenland ice sheet 2. Relationship between dynamics and basal topography, J. Geophys. Res., 106, 33781–33788, doi:10.1029/2001JD900053, 2001. 1042, 1048
Lefebre, F., Gallée, H., van Ypersele, J., and Huybrechts, P.: Modelling of large-scale melt parameters with a regional climate model in south Greenland during the 1991 melt season, Ann. Glaciol., 35, 391–397, doi:10.3189/172756402781816889, 2002. 1044
Letréguilly, A., Reeh, N., and Huybrechts, P.: The Greenland ice sheet through the last glacial-interglacial cycle, Global Planet. Change, 4, 385–394, doi:10.1016/0921-8181(91)90004-G,

TCD
6, 1037–1083, 2012

1991. 1039
Lliboutry, L. and Duval, P.: Various isotropic and anisotropic ices found in glaciers and polar ice caps and their corresponding rheologies, Ann. Geophys., 3, 207–224, 1985, http://www.ann-geophys.net/3/207/1985/. 1042
Ma, Y., Gagliardini, O., Ritz, C., Gillet-Chauvet, F., Durand, G., and Montagnat, M.: Enhancement factors for grounded ice and ice shelves inferred from an anisotropic ice-flow model, J. Glaciol., 56, 805–812, 2010. 1042, 1050
MacAyeal, D. R.: Large-scale ice flow over a viscous basal sediment: theory and application to ice stream B, Antarctica, J. Geophys. Res., 94, 4071–4087, doi:10.1029/JB094iB04p04071, 1989. 1041
Marshall, S. J. and Clarke, G. K. C.: Ice sheet inception: subgrid hypsometric parameterization of mass balance in an ice sheet model, Clim. Dynam., 15, 533–550, doi:10.1007/s003820050298, 1999. 1052
Marsiat, I.: Simulation of the northern hemisphere continental ice sheets over the last glacial-interglacial cycle: experiments with a latitude-longitude vertically integrated ice sheet model coupled to zonally averaged climate model, Paleoclimates, 1, 59–98, 1994. 1047
Marti, O., Braconnot, P., Dufresne, J., Bellier, J., Benshila, R., Bony, S., Brockmann, P., Cadule, P., Caubel, A., Codron, F., Noblet, N., Denvil, S., Fairhead, L., Fichefet, T., Foujols, M., Friedlingstein, P., Goosse, H., Grandpeix, J., Guilyardi, E., Hourdin, F., Idelkadi, A., Kageyama, M., Krinner, G., Lévy, C., Madec, G., Mignot, J., Musat, I., Swingedouw, D., and Talandier, C.: Key features of the IPSL ocean atmosphere model and its sensitivity to atmospheric resolution, Clim. Dynam., 34, 1–26, doi:10.1007/s00382-009-0640-6, 2010. 1043, 1054, 1070
Meehl, G. A., Stocker, T. F., Collins, W. D., Friedlingstein, P., Gaye, A. T., Gregory, J. M., Kitoh, A., Knutti, R., Murphy, J. M., Noda, A., Raper, S. C. B., Watterson, I. G., Weaver, A. J., and Zhao, Z.-C.: Global climate projections, in: Climate Change 2007: The Physical Science Basis. Contribution of Working Group I to the Fourth Assessment Report of the Intergovernmental Panel on Climate Change, (edited by: Solomon, S., Qin, D., Manning, M., Chen, Z., Marquis, M., Averyt, K. B., Tignor, M., and Miller, H. L.), Cambridge Univ. Press, 2007. 1038
Otto-Bliesner, B. L., Marshall, S. J., Overpeck, J. T., Miller, G. H., and Hu, A.: Simulating Arctic climate warmth and icefield retreat in the last interglaciation, Science, 311, 1751–1753, 2006. 1060

TCD
6, 1037–1083, 2012

Peyaud, V., Ritz, C., and Krinner, G.: Modelling the Early Weichselian Eurasian Ice Sheets: role of ice shelves and influence of ice-dammed lakes, Clim. Past, 3, 375–386, doi:10.5194/cp-3-375-2007, 2007. 1041, 1046, 1047

Philippon, G., Ramstein, G., Charbit, S., Kageyama, M., Ritz, C., and Dumas, C.: Evolution of the Antarctic ice sheet throughout the last deglaciation: a study with a new coupled climate – north and south hemisphere ice sheet model, Earth Planet. Sci. Lett., 248, 750–758, doi:10.1016/j.epsl.2006.06.017, 2006. 1041

Pollard, D.: A retrospective look at coupled ice sheet-climate modeling, Clim. Change, 100, 173–194, doi:10.1007/s10584-010-9830-9, 2010. 1039

Reeh, N.: Parameterization of melt rate and surface temperature on the Greenland Ice Sheet, Polarforschung, 59, 113–128, 1991. 1046, 1047

Ridley, J., Gregory, J., Huybrechts, P., and Lowe, J.: Thresholds for irreversible decline of the Greenland ice sheet, Clim. Dynam., 35, 1049–1057, doi:10.1007/s00382-009-0646-0, 2010. 1039

Ridley, J. K., Huybrechts, P., Gregory, J. M., and Lowe, J. A.: Elimination of the Greenland Ice Sheet in a high CO_2 climate, J. Climate, 18, 3409–3427, doi:10.1175/JCLI3482.1, 2005. 1039

Ritz, C., Lliboutry, L., and Rado, C.: Analysis of a 870 m deep temperature profile at Dome C, Ann. Glaciol., 3, 284–289, 1983. 1042

Ritz, C., Fabre, A., and Letréguilly, A.: Sensitivity of a Greenland ice sheet model to ice flow and ablation parameters: consequences for the evolution through the last climatic cycle, Clim. Dynam., 13, 11–23, doi:10.1007/s003820050149, 1997. 1039, 1044, 1048

Ritz, C., Rommelaere, V., and Dumas, C.: Modeling the evolution of Antarctic ice sheet over the last 420,000 years: Implications for altitude changes in the Vostok region, J. Geophys. Res., 106, 31943–31964, 2001. 1039, 1041

Robinson, A., Calov, R., and Ganopolski, A.: Greenland ice sheet model parameters constrained using simulations of the Eemian Interglacial, Clim. Past, 7, 381–396, doi:10.5194/cp-7-381-2011, 2011. 1038, 1060

Salas-Mélia, D., Chauvin, F., Déqué, M., Douville, H., Gueremy, J. F., Marquet, P., Planton, S., Royer, J. F., and Tyteca, S.: Description and validation of the CNRM-CM3 global coupled model, CNRM working note, 103, 36 pp., 2005. 1043, 1070

Shapiro, N. M. and Ritzwoller, M. H.: Inferring surface heat flux distributions guided by a global seismic model: particular application to Antarctica, Earth Planet. Sci. Lett., 223, 213–224,

TCD
6, 1037–1083, 2012

doi:10.1016/j.epsl.2004.04.011, 2004. 1042, 1061
Sjolte, J., Hoffmann, G., Johnsen, S., Vinther, B., Masson-Delmotte, V., and Sturm, C.: Modeling the water isotopes in Greenland precipitation 1959–2001 with the meso-scale model REMO-iso, J. Geophys. Res., 116, D18105, doi:10.1029/2010JD015287, 2011. 1044
Solgaard, A. M. and Langen, P. L.: Multistability of the Greenland ice sheet and the effects of an adaptive mass balance formulation, Clim. Dynam., doi:10.1007/s00382-012-1305-4, in press, 2012. 1060
Steffen, K., Box, J., and Abdalati, W.: Greenland Climate Network: GC-Net, Special report on glaciers, ice sheets and volcanoes, (edited by: Colbeck, W. C.), Report 96-27103, 98–103, 1996. 1053, 1078, 1079
Stokes, C. R. and Clark, C. D.: Geomorphological criteria for identifying Pleistocene ice streams, Ann. Glaciol., 28, 67–74, 1999. 1041
Stone, E. J., Lunt, D. J., Rutt, I. C., and Hanna, E.: Investigating the sensitivity of numerical model simulations of the modern state of the Greenland ice-sheet and its future response to climate change, The Cryosphere, 4, 397–417, doi:10.5194/tc-4-397-2010, 2010. 1039, 1060
Sturm, K., Hoffmann, G., Langmann, B., and Stichler, W.: Simulation of ^{18}O in precipitation by the regional circulation model REMOiso, Hydrol. Proces., 19, 3425–3444, doi:10.1002/hyp.5979, 2005. 1044, 1070
Swingedouw, D., Fichefet, T., Huybrechts, P., Goosse, H., Driesschaert, E., and Loutre, M.: Antarctic ice-sheet melting provides negative feedbacks on future climate warming, Geophys. Res. Lett., 35, L17705, doi:10.1029/2008GL034410, 2008. 1039
Tarasov, L. and Peltier, W. R.: Greenland glacial history and local geodynamic consequences, Geophys. J. Int., 150, 198–229, doi:10.1046/j.1365-246X.2002.01702.x, 2002. 1039
Uppala, S. M., Kållberg, P. W., Simmons, A. J., Andrae, U., Bechtold, V. D. C., Fiorino, M., Gibson, J. K., Haseler, J., Hernandez, A., Kelly, G. A., Li, X., Onogi, K., Saarinen, S., Sokka, N., Allan, R. P., Andersson, E., Arpe, K., Balmaseda, M. A., Beljaars, A. C. M., Berg, L. V. D., Bidlot, J., Bormann, N., Caires, S., Chevallier, F., Dethof, A., Dragosavac, M., Fisher, M., Fuentes, M., Hagemann, S., Hólm, E., Hoskins, B. J., Isaksen, L., Janssen, P. A. E. M., Jenne, R., McNally, A. P., Mahfouf, J.-F., Morcrette, J.-J., Rayner, N. A., Saunders, R. W., Simon, P., Sterl, A., Trenberth, K. E., Untch, A., Vasiljevic, D., Viterbo, P., and Woollen, J.: The ERA-40 re-analysis, Q. J. Roy. Meteor. Soc., 131, 2961–3012, doi:10.1256/qj.04.176, 2005. 1044, 1070

TCD
6, 1037–1083, 2012

van den Broeke, M., Smeets, P., Ettema, J., and Munneke, P. K.: Surface radiation balance in the ablation zone of the west Greenland ice sheet, J. Geophys. Res., 113, D13105, doi:10.1029/2007JD009283, 2008. 1040

van den Broeke, M., Bus, C., Ettema, J., and Smeets, P.: Temperature thresholds for degree-day modelling of Greenland ice sheet melt rates, Geophys. Res. Lett., 37, L18501, doi:10.1029/2010GL044123, 2010. 1046, 1047

van der Veen, C. J., Bromwich, D. H., Csatho, B. M., and Kim, C.: Trend surface analysis of Greenland accumulation, J. Geophys. Res., 106, 33909–33918, doi:10.1029/2001JD900156, 2001. 1054, 1055, 1061, 1080

Vizcaíno, M., Mikolajewicz, U., Gröger, M., Maier-Reimer, E., Schurgers, G., and Winguth, A. M. E.: Long-term ice sheet-climate interactions under anthropogenic greenhouse forcing simulated with a complex Earth System Model, Clim. Dynam., 31, 665–690, doi:10.1007/s00382-008-0369-7, 2008. 1039

Vizcaíno, M., Mikolajewicz, U., Jungclaus, J., and Schurgers, G.: Climate modification by future ice sheet changes and consequences for ice sheet mass balance, Clim. Dynam., 34, 301–324, doi:10.1007/s00382-009-0591-y, 2010. 1039

Yoshimori, M. and Abe-Ouchi, A.: Sources of spread in multi-model projections of the Greenland ice-sheet surface mass balance, J. Climate, doi:10.1175/2011JCLI4011.1, 2012. 1038, 1043

TCD
6, 1037–1083, 2012

Table 1. Main characteristics of atmospheric datasets used for this study. Resolutions in ° approximated. *: for RACMO2/GR.

Dataset	Atmosphere resolution	Lateral bounds	Ocean bound. Conditions	Reference
Fausto/Ettema FE09	Fausto (t2m), RACMO2/GR (precip.), 0.29° × 0.29°, L40*	ERA40*	obs. derived ERA40*	Fausto et al. (2009) Ettema et al. (2009)
ERA-40	ERA40, 1.125° × 1.125°, T159 L60	–	obs. derived HadISST/NCEP	Uppala et al. (2005)
MAR	MAR, 0.66° × 0.66°	ERA40	obs. derived ERA40	Fettweis (2007)
REMO	REMO, 0.5° × 0.5°, L19	ECHAM4	obs. derived ERA40	Sturm et al. (2005)
LMDZ-zoom	LMDZ4, 1.2–3.6° × 0.5–5.5°, L19	–	obs. derived AMIP2	Krinner and Genthon (1998)
LMDZ-SISVAT	LMDZ4, 3.75° × 2.5°, L19	–	obs. derived AMIP2	
IPSL-CM4	LMDZ4, 3.75° × 2.5°, L19	–	coupled ORCA model	Marti et al. (2010)
CNRM-CM3.3	ARPEGE-Climat 3 1, 9° × 1.9°, T63 L45	–	coupled OPA 8 model	Salas-Mélia et al. (2005)

TCD
6, 1037–1083, 2012

Table 2. Model parameters used in the GRISLI model for this study.

Variable	Identifier name	Value
Basal drag coefficient	β	1500 m yr Pa^{-1}
SIA enhancement factor, Glen	E_3^{SIA}	3
SIA enhancement factor, linear	E_1^{SIA}	1
SSA enhancement factor, Glen	E_3^{SSA}	0.8
SSA enhancement factor, linear	E_1^{SSA}	1
Transition temperature of deformation, Glen	T_3^{trans}	−6.5 °C
Activation energy below transition, Glen	Q_3^{cold}	7.820×10^4 J mol^{-1}
Activation energy above transition, Glen	Q_3^{warm}	9.545×10^4 J mol^{-1}
Transition temperature of deformation, linear	T_1^{trans}	−10 °C
Activation energy below transition, linear	Q_1^{cold}	4.0×10^4 J mol^{-1}
Activation energy above transition, linear	Q_1^{warm}	6.0×10^4 J mol^{-1}
Topographic lapse rate, July	lr_{july}	5.426 °C km^{-1}
Topographic lapse rate, annual	lr_{ann}	6.309 °C km^{-1}
Precipitation ratio parameter	γ	0.07 °C^{-1}
PDD standard deviation of daily temperature	σ	5.0 °C
PDD ice ablation coefficient	C_{ice}	8.0 mm day^{-1} °C^{-1}
PDD snow ablation coefficient	C_{snow}	5.0 mm day^{-1} °C^{-1}

TCD
6, 1037–1083, 2012

Table 3. Large scale biases of atmospheric datasets in respect to FE09, and key variable explaining the deviation of volume (bold).

Atmospheric dataset	Anomaly of temperature and precipitation South	Anomaly of temperature and precipitation North
ERA40	**Warm**	**Warm**
MAR	Warm and **dry**	Cold and wet
REMO	Warm and wet	**Warm** and wet
LMDZZ	**Dry**	**Warm**
LMDZSV	Warm and wet	Warm and wet
IPSL	Cold and **dry**	Cold and dry
CNRM	**Strongly warm** and wet	**Strongly cold** and dry

TCD
6, 1037–1083, 2012

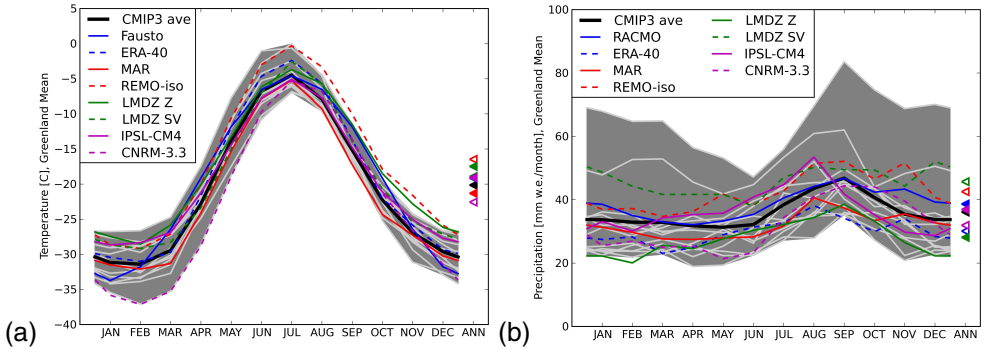

Fig. 1. Greenland mean seasonal cycle of near surface air temperature (in ˚C, left panel) and precipitation (in mm of water equivalent per month, right panel) for the 8 forcing datasets used in this study (colored lines). Annual mean values are symbolised by triangles on the right. The grey, shaded area is the spread of 12 CMIP-3 models. Light grey and black lines, respectively represent individual models and their mean.

TCD
6, 1037–1083, 2012

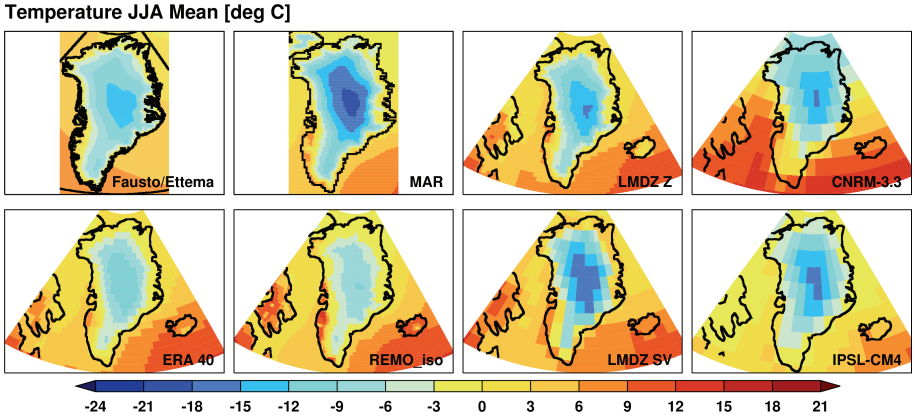

Fig. 2. Climatological (1980–1999) June-July-August mean 2 m temperature in the eight different climate models (in °C).

TCD
6, 1037–1083, 2012

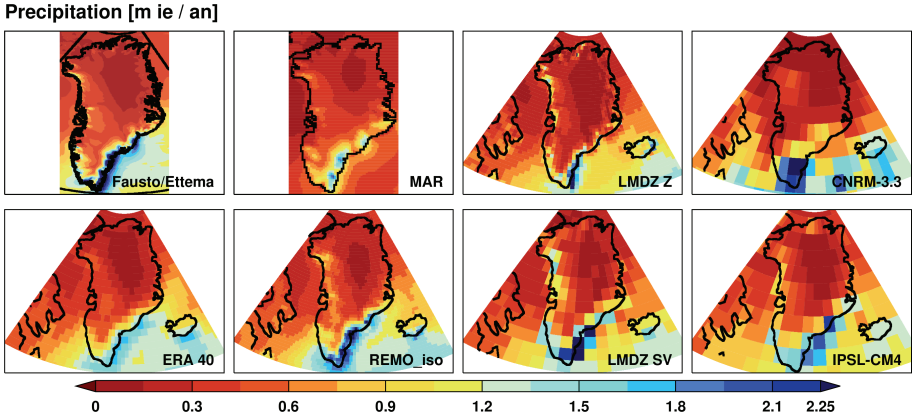

Fig. 3. Climatological (1980–1999) annual mean precipitation (solid+liquid) in the eight different climate models (in meter of ice equivalent).

TCD
6, 1037–1083, 2012

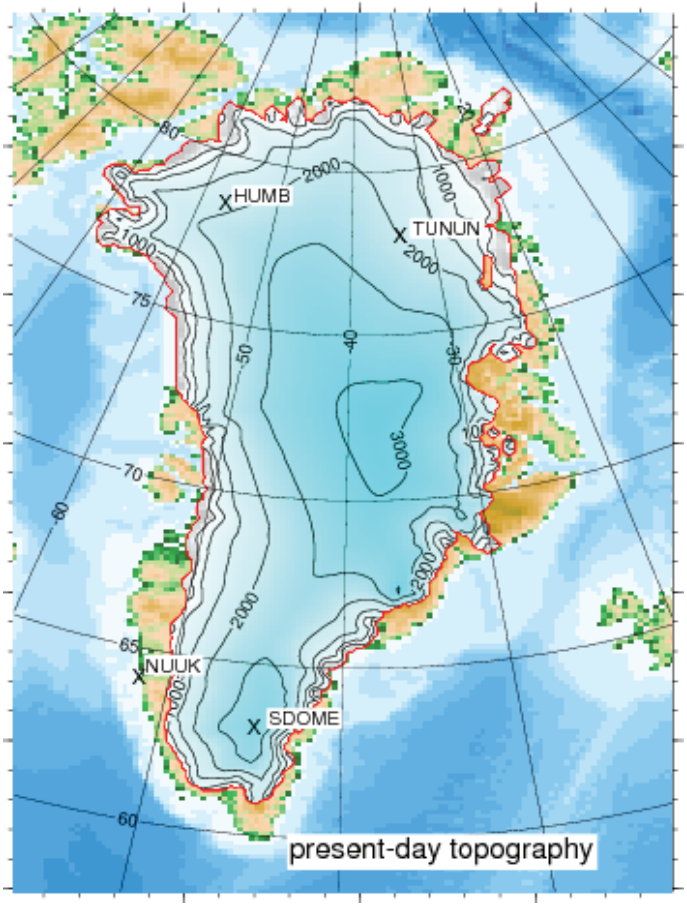

Fig. 4. Present day topography of the GIS with selected weather stations.

TCD
6, 1037–1083, 2012

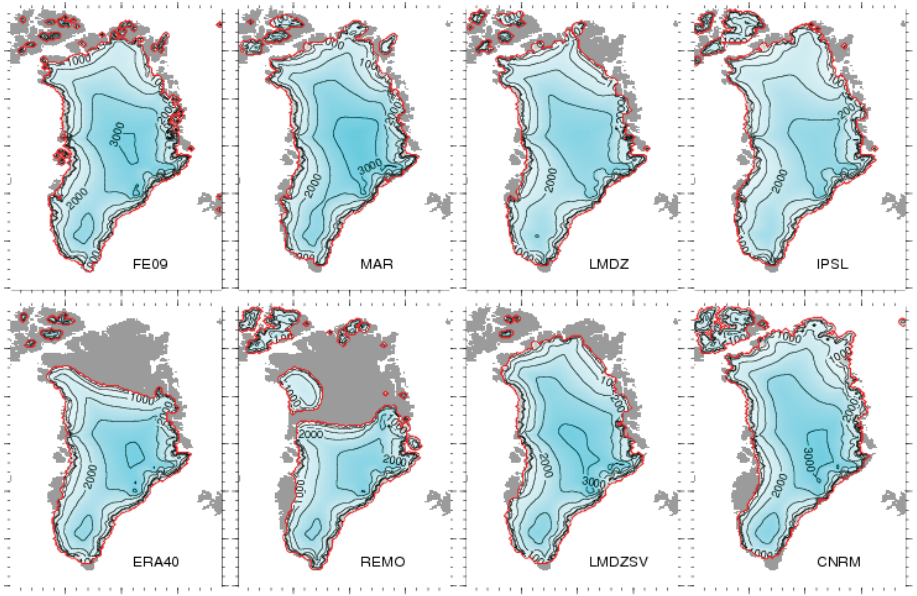

Fig. 5. Simulated topographies at the end of the 20 kyr climatic steady state experiment.

TCD
6, 1037–1083, 2012

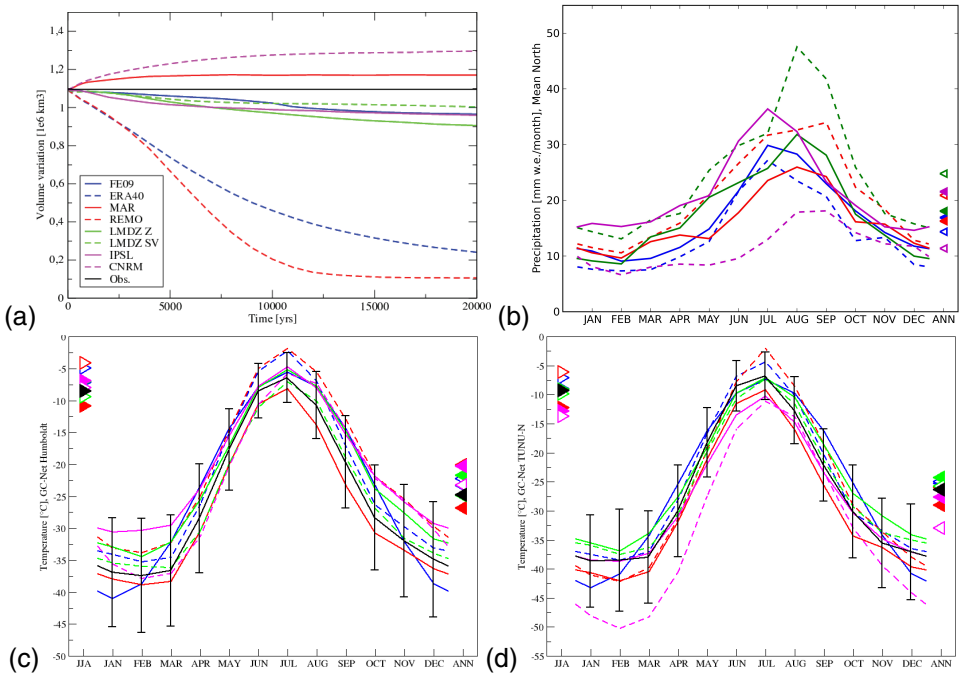

Fig. 6. North Greenland (latitude greater than 75° N) simulated ice volume evolution for each individual atmospheric model **(a)**. Regional monthly mean precipitation for each individual atmospheric model **(b)**, with annual mean values (triangles). Near surface air temperature of each individual atmospheric model and station climatology for Humboldt **(c)** and Tunu-N **(d)** (Steffen et al., 1996), with July temperature (left hand triangles) and annual mean temperature (right hand triangles). The black markers stand for the observations (initial regional ice volume and t2m stations measurement).

TCD
6, 1037–1083, 2012

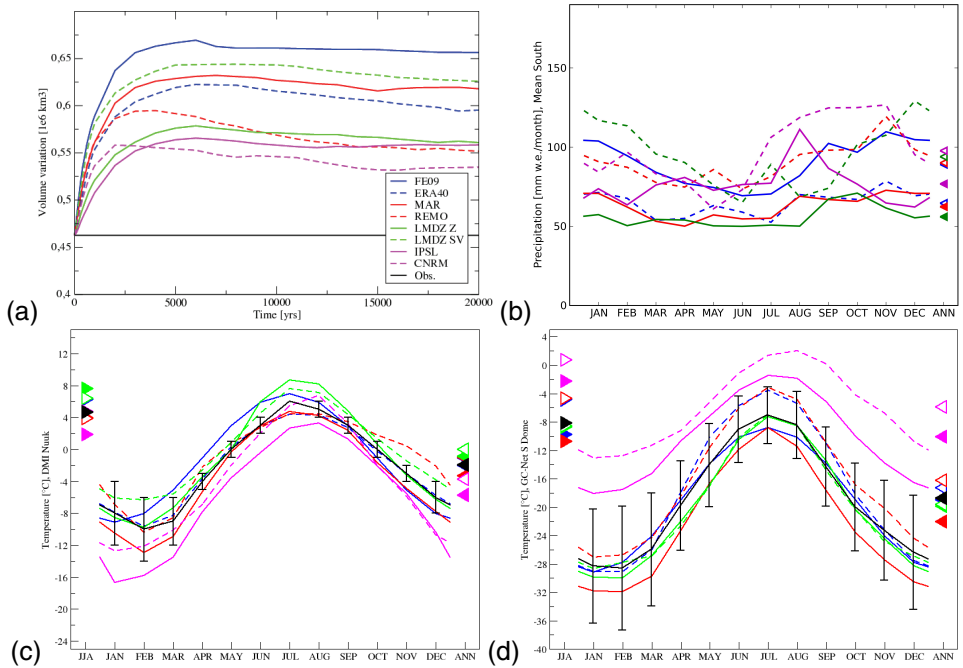

Fig. 7. South (latitude lower than 68° N) simulated volume evolution for each individual atmospheric model **(a)**. Regional monthly mean precipitation for each individual atmospheric model **(b)**, with annual mean values (triangles). Near surface air temperature of each individual atmospheric model and station climatology for Nuuk **(c)** (DMI) and South Dome **(d)** (Steffen et al., 1996), with July temperature (left-sided triangles) and annual mean temperature (right-sided triangles). The black markers stand for the observations (initial regional ice volume and t2m stations measurement).

TCD
6, 1037–1083, 2012

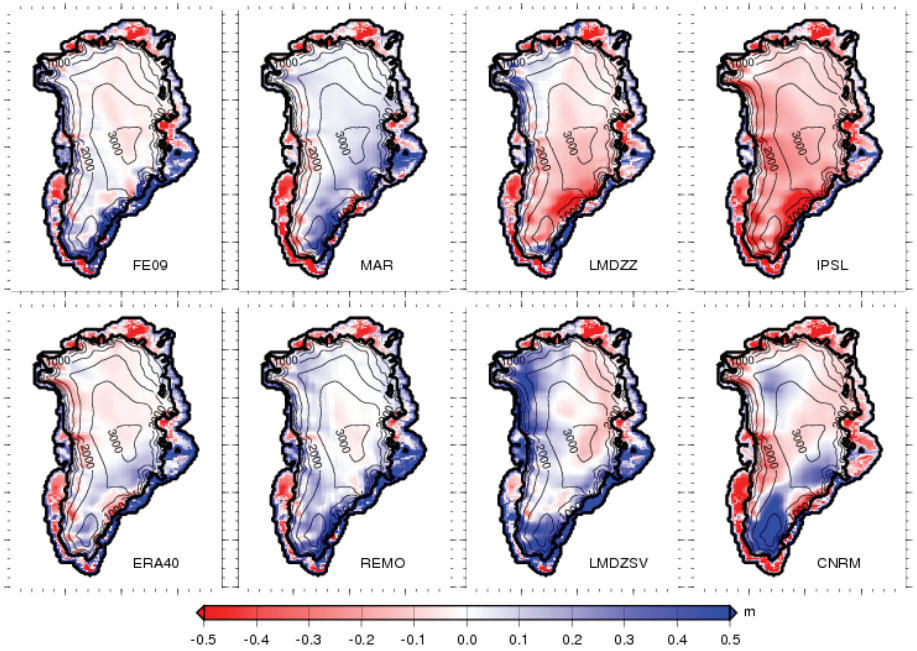

Fig. 8. Annual accumulation differences between ISM evaluation and observations field-based (Burgess et al., 2010; van der Veen et al., 2001) for each individual atmospheric dataset.

TCD
6, 1037–1083, 2012

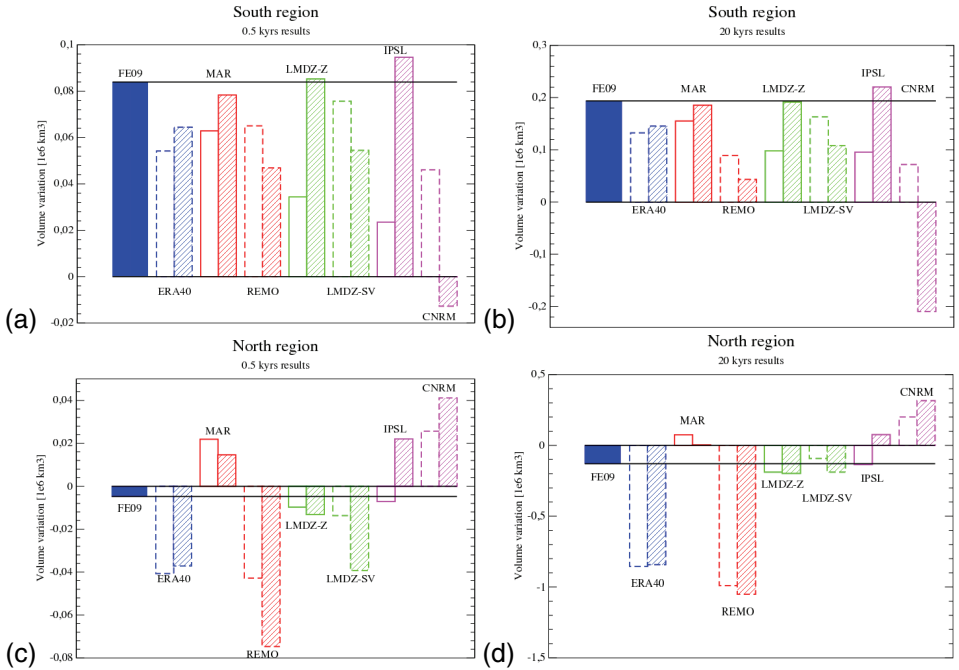

Fig. 9. Regional volume variation (simulated volume minus initial volume) for each model. Empty bars correspond to the standard volume variation (dV_i) and hatched bars correspond to the Ettema et al. (2009) precipitation map volume variation (dV_i'). The simulated reference volume corresponds to the first bar (dV_0, FE09). The upper panel corresponds to the South region (latitude lower than 68° N) at 0.5 kyr (a) and 20 kyr (b), and the lower panel corresponds to the North region (latitude greater than 75° N) at 0.5 kyr (c) and 20 kyr (d).

TCD
6, 1037–1083, 2012

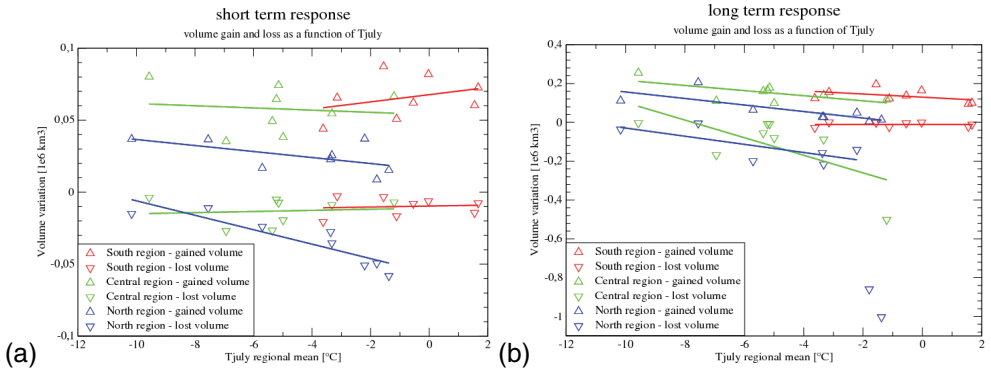

Fig. 10. Volume loss (down-pointing triangle) and gain (up-pointing triangle) as a function of July mean temperature. The tendency lines are also plotted (we omitted the two warmest models, ERA40 and REMO, for the tendency of the North volume loss on the long-term response). The lost (resp. gained) volume is defined as the sum of the negative (resp. positive) thickness variation multiplied by the ISM grid cell area. On the left, the volume deviations after 500 yr simulation and, on the right, after 20 kyr simulation. Each pair of traingles (down and up-pointing) represent a particular atmospheric model.

TCD
6, 1037–1083, 2012

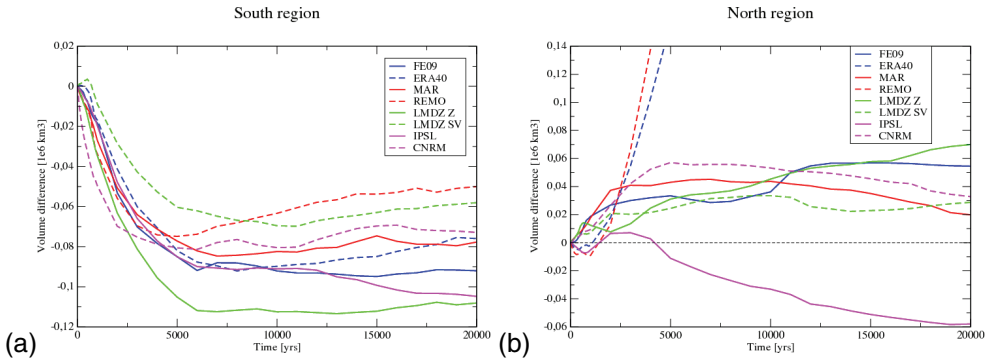

Fig. 11. Evolution of the difference between the no-lapse rate experiment minus the standard correction experiment. On the left, the South region (latitude lower than 68° N) and on the right, the North region (latitude greater than 75° N).

TCD
6, 1037–1083, 2012